Middle-atmospheric response to a future increase in humidity arising from increased methane abundance

Middle-atmospheric response to a future increase in humidity arising from increased methane abundance

I. A. MacKenzie and R. S. Harwood

Institute of Atmospheric and Environmental Science, University of Edinburgh, Edinburgh, UK

Received 12 March 2003; revised 17 October 2003; accepted 30 October 2003; published 27 January 2004.

[1] The response of the middle atmosphere to an increase in humidity arising from a possible future increase in CH_4 is examined in a general circulation model with interactive H_2O and O_3. A chemical parameterization allows the middle-atmospheric H_2O change to evolve naturally from an imposed change in tropospheric CH_4. First, a simulation of the year 2060 using postulated loadings of the radiatively active gases is compared with a control simulation of the present-day atmosphere. Then, the particular contribution of the CH_4 (and hence H_2O) change to the observed difference is isolated by repeating the 2060 simulation without the projected CH_4 change. Under the Intergovernmental Panel on Climate Change Special Report on Emission Scenarios (SRES) B2 scenario, the middle atmosphere in 2060 cools by up to $\sim$5 K relative to 1995, with the CH_4-derived increase in H_2O accounting for $\sim$10% of the change. The cooling is accompanied by a strengthened general circulation, intensified dynamic heating rates, and a reduction in the mean age of middle-atmospheric air. The component of the circulation change attributable solely to the H_2O change differs somewhat from the net response: The H_2O change causes a greater increase in the descent rate in the north than in the south, ages the stratospheric air, and has a distinct effect on age/N_2O correlations. Around 20% of the increased prevalence of polar stratospheric clouds (PSCs) in 2060 is due to the microphysical effect of the extra H_2O, with the remainder attributable to the reduced vortex temperatures. Although the PSC increase facilitates release of reactive chlorine, this positive impact on chemical O_3 destruction is outweighed by the negative impact of the reduced total chlorine in 2060. Nonetheless, the H_2O increase does make the 2060 Arctic O_3 loss $\sim$15% greater than it would otherwise be. *INDEX TERMS:* 0325 Atmospheric Composition and Structure: Evolution of the atmosphere; 0340 Atmospheric Composition and Structure: Middle atmosphere—composition and chemistry; 0341 Atmospheric Composition and Structure: Middle atmosphere—constituent transport and chemistry (3334); 1610 Global Change: Atmosphere (0315, 0325); 3334 Meteorology and Atmospheric Dynamics: Middle atmosphere dynamics (0341, 0342); *KEYWORDS:* climate, middle atmosphere, water vapor

Citation: MacKenzie, I. A., and R. S. Harwood (2004), Middle-atmospheric response to a future increase in humidity arising from increased methane abundance, *J. Geophys. Res.*, *109*, D02107, doi:10.1029/2003JD003590.

1. Introduction

[2] Water (H_2O) vapor in the middle atmosphere is active radiatively, chemically, and physically; thus a change in its abundance has a number of potential impacts. Radiatively, the presence of H_2O helps determine the temperature, and hence the circulation, of the stratosphere and mesosphere by contributing to their long-wave cooling. Chemically, H_2O is the primary source of OH radicals, which are central to much stratospheric chemistry. Physically, the H_2O concentration determines the temperature at which polar stratospheric clouds (PSCs) can form, and thus modulates the severity of polar ozone (O_3) destruction.

[3] The abundance of H_2O in the middle atmosphere is controlled by two main factors: the rate of transport of H_2O from the troposphere and the rate of in-situ chemical production of H_2O from the oxidation of methane (CH_4), which is also transported from the troposphere. Air entering the stratosphere is, it is believed, freeze dried by its passage through the cold tropical tropopause, and consequently arrives with a relatively low H_2O content of the order of 2 to 3 parts per million by volume (ppmv), compared with the hundreds of ppmv found in the troposphere. The precise mixing ratio in the incoming air is highly sensitive to tropopause temperature, as shown by the so-called tape recorder effect where the annual cycle in tropical tropopause temperature is imprinted on the H_2O content of the air above [*Mote et al.*, 1996]. Owing to the source from CH_4 oxidation, the mixing ratio of H_2O increases steadily with height from the tropopause up to the lower mesosphere where it peaks currently at around 6 ppmv. At greater heights, the photolytic destruction of H_2O becomes dominant and the abundance falls sharply.

0148-0227/04/2003JD003590

[4] Since CH_4 oxidation presently contributes approximately half of the peak H_2O abundance in the middle atmosphere, it follows that any significant change in tropospheric CH_4 abundance will, in turn, cause a significant change in middle-atmospheric H_2O. Several studies have observed an upward trend in stratospheric H_2O over the past few decades [e.g., *Rosenlof et al.*, 2001; *Oltmans et al.*, 2000] with a mean increase of around 0.05 ppmv yr^{-1} recorded between 100 and 10 hPa. This rise has not been fully explained, but some 40% of it is attributed to increasing CH_4 entering from the troposphere. Tropospheric CH_4 has increased primarily as a result of increased emission at the Earth's surface, with a possible smaller role for reduced chemical loss. Anthropogenic sources currently constitute $\sim$60% of the total CH_4 emission, and this contribution is likely to increase over the coming century [*Intergovernmental Panel on Climate Change* (*IPCC*), 2001]. The climatic implications of changing concentrations of radiatively active gases is a subject of much current interest, and the role of H_2O in the middle atmosphere, where it is the next most important radiating gas after CO_2, has been the focus of a number of recent studies. Results suggest that increasing H_2O has made a significant contribution to the recent downward trend in stratospheric temperatures [*Forster and Shine*, 1999; *Smith et al.*, 2001; *Oinas et al.*, 2001], and that further cooling from the same source might play an important role in future climate change and ozone evolution [*Dvortsov and Solomon*, 2001; *Shindell*, 2001]. The specific radiative response to an imposed perturbation of middle-atmospheric H_2O is, however, highly sensitive to the altitude range over which the change is applied [*Forster and Shine*, 2002]. Moreover, the initial radiative response induces a complex dynamic reaction which can feed back onto the radiation through the atmospheric transport. Full elucidation of these processes requires the application of self-consistent three-dimensional models.

[5] The study presented here uses a comprehensive general circulation model (GCM) to examine the response of the middle atmosphere to a humidity increase attributable directly to a postulated change in tropospheric CH_4 between the present day and the year 2060. The sensitivity to CH_4 changes is thus examined in isolation from other less established contributions to the H_2O trend. The inclusion of a parameterized and interactive $CH_4/H_2O/H_2$ chemistry scheme in the GCM allows the middle-atmospheric H_2O change to evolve naturally from the imposed CH_4 change and thus consistently with model's dynamics and transport. A simplified treatment of polar ozone chemistry affords an insight into its sensitivity to the adjusted CH_4. The experiment uses present-day sea surface temperatures (SSTs), but is conducted against the background of the expected changes in the other long-lived, radiatively active gases.

2. Model Description

[6] The dynamic model used was the Met Office Unified Model (UM) [*Cullen*, 1993], a hydrostatic, primitive-equation, grid-point model with hybrid vertical coordinates. Versions of this model, with and without chemistry, have been used in a number of other stratospheric climate studies examining the response to past and projected trends in the radiatively active gases [*Butchart et al.*, 2000; *Austin et al.*, 2000, 2001; *Austin*, 2002]. The model configuration used for this study, focusing on the role of CH_4/H_2O change, had 64 levels extending from the surface to 0.01 hPa ($\sim$80 km) with a vertical resolution in the middle atmosphere of $\sim$1.3 km. The horizontal resolution was 3.75° longitude by 2.5° latitude. Radiative heating rates were calculated using the scheme of *Edwards and Slingo* [1996] with some modifications in the middle atmosphere [*Zhong and Haigh*, 2001]. The gases treated by the scheme are CO_2, H_2O, O_3, O_2, N_2O, CH_4, CFC-11, and CFC-12; all of these except CO_2, O_2, and the CFCs were advected and interactive with the parameterized chemistry described in the next section. A development of the Edwards-Slingo scheme by *Cusack et al.* [1998] to account for the absorption of background aerosols was also included. The model's primary variables, and additional tracers, were advected by a conservative, flux-based, finite volume scheme. The moisture content of air passing from the troposphere to the stratosphere was capped at the saturation vapor pressure calculated using the Goff-Gratch formula. An orographic gravity-wave drag (gwd) scheme *Gregory et al.* [1998] operated from the ground up to 20 hPa, where it was replaced by Rayleigh friction (RF). Recent work has shown that inclusion of a nonorographic gwd scheme instead of RF brings the model's stratospheric temperatures and transport somewhat closer to reality [*Austin et al.*, 2003]. Nevertheless, use of RF is unlikely to greatly influence the model's sensitivity to changes in the radiative environment because the flow is forced mainly by internally generated waves. Other physical parameterizations within the model largely followed the HADAM3 package [*Pope et al.*, 2000].

3. Chemical Parameterizations

3.1. Water Vapor, Methane, and Hydrogen

[7] Three advected tracers are used to represent H_2O, CH_4, and H_2. For H_2O the model's specific humidity field is used; CH_4 and H_2 are added to the model as additional tracers. The chemical treatment of these species is based on the descriptions of their middle-atmospheric chemistry given by *Le Texier et al.* [1988] and *Hurst et al.* [1999]. In the stratosphere, it is assumed that H_2O is produced from CH_4 but is not destroyed, whereas in the mesosphere H_2O is destroyed but not produced. In the troposphere, all species are advected without chemistry; H_2O participates in the model's hydrological cycle, while CH_4 is entirely passive and is held at a fixed, globally uniform, mixing ratio at the lower boundary.

3.1.1. Stratosphere

[8] Oxidation of CH_4 arriving from the troposphere is the principal chemical source of H_2O in the stratosphere. In reality, the oxidation process is complex: CH_4 reacts with OH, O^1D, or Cl initiating a sequence of further reactions which, via a variety of routes, lead ultimately to $2H_2O$ and CO. A reaction branch producing the long-lived species H_2 reduces the immediate yield of H_2O per CH_4 molecule oxidized to a number somewhat less than two. However, stratospheric H_2 (which is mostly of tropospheric origin) is itself oxidized to H_2O; and it so happens that the rate of H_2O production from H_2 almost exactly balances the rate of H_2 production from CH_4 in the lower and middle stratosphere. Consequently, the H_2 content of a given air parcel is

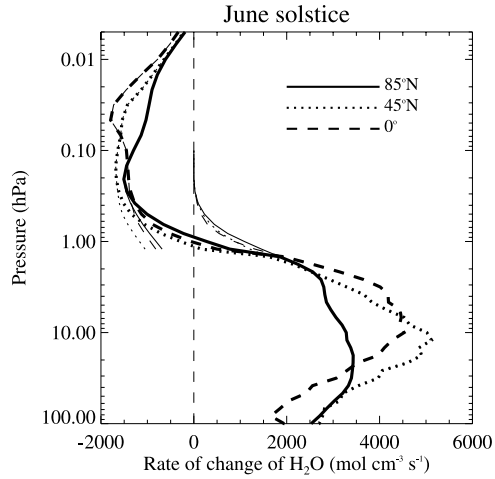

Figure 1. Chemical rate of change of H_2O as a function of height. Obtained from the pseudo rate coefficients for the oxidation of CH_4 and the calculated photolysis coefficients for H_2O acting on climatological profiles of these two species. The thin lines show the rate of H_2O production from CH_4 in the stratosphere and lower mesosphere and the rate of photolytic destruction of H_2O in the mesosphere and upper stratosphere. The thick lines show the net rate of change of H_2O due to these two processes combined and overlie the thin lines everywhere except for a region around 1 hPa, where the H_2O production and destruction processes have similar magnitudes. Results are shown for three separate latitudes.

near constant with time. Thus H_2 originating from the troposphere and from CH_4 oxidation is treated implicitly in the parameterization by assuming that the conversion of CH_4 to H_2O takes place by a single pseudo reaction $CH_4 \xrightarrow{k} 2H_2O$.

[9] The rate coefficient k for the pseudo reaction is calculated from the Thin Air two-dimensional photochemical model [*Kinnersley and Harwood*, 1993] as a function of season, latitude and height using the expression

$$k = 0.5(d[H_2O]/dt)/[CH_4]$$

[10] Comparison of the rates of change of H_2O and CH_4 within the two-dimensional model confirms that the ratio $[dH_2O/dt]/[-dCH_4/dt]$ departs significantly from 2 only where the rate of change of the two species is low. Observations of H_2O and CH_4 from aircraft and from space [*Hurst et al.*, 1999; *Abbas et al.*, 1996] also imply a ratio close to 2 in the middle and lower stratosphere.

[11] H_2 produced in the mesosphere from photolysis of H_2O (see next section) is assumed to oxidize in the stratosphere at the same rate as CH_4. The chemical continuity equations then become

$$d[H_2O]/dt = 2k[CH_4] + k[H_2]$$

$$d[CH_4]/dt = -k[CH_4]$$

$$d[H_2]/dt = -k[H_2]$$

The species concentrations are advanced by solving this linear system of equations using an implicit time stepping method.

[12] In addition to the chemical treatment of stratospheric water vapor, a simple treatment of the sedimentation of water-ice PSCs is also implemented. Wherever the H_2O mixing ratio poleward of 45° exceeded the saturated vapor pressure of water over ice, the frozen fraction was allowed to fall out with a velocity of 1.2 km d^{-1}. Sedimentation of hydrated-HNO_3 PSCs was not treated.

3.1.2. Mesosphere

[13] In the mesosphere, both H_2O and CH_4 are assumed to be destroyed by photolysis with no production terms

$$d[H_2O]/dt = -J_{H_2O}[H_2O]$$

$$d[CH_4]/dt = -J_{CH_4}[CH_4]$$

[14] For H_2O, absorption at the Lyman α frequency and in the Schumann Runge bands is taken into account. For CH_4 only the Lyman α is considered. The photolysis coefficients $J_{H_2}O$ and J_{CH_4} are calculated as a function of solar zenith angle and pressure using a precalculated look-up table of the slant column of O_2. In the Lyman α region the parameterization of *Chabrillat and Kockarts* [1997] is used, assuming a quiet-sun irradiance of 3×10^{11} photons cm^{-2} s^{-1} at the top of the atmosphere, and mean absorption cross sections of 1.5×10^{11} and 1.9×10^{11} cm^{-2} for H_2O and CH_4, respectively. Photolysis coefficients for H_2O in the Schumann Runge bands were calculated by the opacity distribution function method [*Minschwaner et al.*, 1993; *Siskind et al.*, 1994]. The hydrogen liberated by H_2O photolysis is assumed to be rapidly converted into H_2, and this H_2 is available for re-conversion to H_2O when it enters the stratosphere. The photolysis products of CH_4 are insignificant for the hydrogen budget of the middle atmosphere and are disregarded.

[15] Figure 1 shows the rates of change of H_2O obtained by combining the rate coefficients for CH_4 oxidation and for H_2O photolysis with climatological profiles of CH_4 and H_2O. The change from net production of H_2O to net loss takes place just above 1 hPa. The switch from the stratospheric to the mesospheric parameterization is therefore made at this altitude with one transition model level, where the chemical rate of change of H_2O is assumed to be zero.

3.2. Nitrous Oxide

[16] N_2O is treated similarly to CH_4. In the troposphere it is assumed passive and is subject to a globally uniform, surface boundary condition. In the middle atmosphere it decays at a rate proportional to its concentration with the rate coefficient derived from the two-dimensional model as a function of season, latitude and height, i.e., $k = (-d[N_2O]/dt)/[N_2O]$.

3.3. Ozone, PSCs, and Reactive Chlorine

[17] The ozone parameterization uses the scheme of *Cariolle and Deque* [1986]. This calculates the local rate of ozone change as a function of season, ozone mixing ratio, overhead ozone column, and temperature. For this study, a simple treatment of PSC-initiated ozone loss was added to the basic scheme, adapted from the method described by

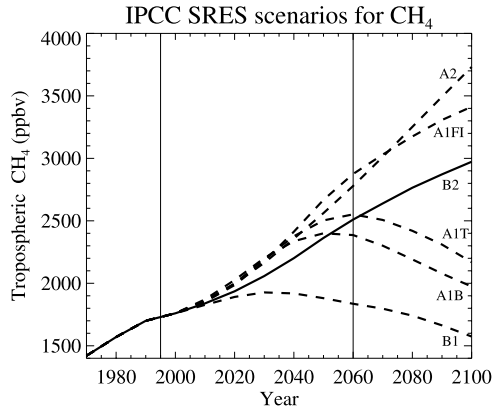

Figure 2. Trends in tropospheric CH_4 calculated from the IPCC SRES marker/illustrative emission scenarios. The B2 scenario used for this experiment is shown as a solid line, and the other scenarios are dashed lines. Thin vertical lines mark the simulated years, 1995 and 2060. Based on data published by *IPCC* [2001, Appendix II].

Braesicke and Pyle [2003]. A threshold temperature for PSC formation is calculated at each time step for each grid point in the extra-tropical lower stratosphere using the mixing ratio of the H_2O-tracer and the algorithm of *Carslaw et al.* [1995] to identify the temperature at which H_2SO_4 aerosols begin to grow rapidly by uptake of HNO_3. (Mixing ratios of 10 ppmv, and 0.5 ppbv were assumed for HNO_3 and H_2SO_4 respectively.) No distinction is made between different PSC types. Air masses are assigned, on the basis of their history, a normalized "chlorine activation" index Cl_i which reflects the degree to which the chlorine in the air has been activated by contact with PSCs. Cl_i has a positive tendency of time constant 4 hours wherever the air temperature is below the PSC threshold, and an omnipresent, temperature-insensitive, negative tendency, of time constant 5 days in the Northern Hemisphere and 10 days in the Southern Hemisphere. The PSC-initiated ozone loss rate is then expressed as $d[O_3]/dt = k\ Cl_i\ [O_3]$. Runs with present-day CFC loadings used a reaction coefficient, k of 10 d^{-1}, whereas those runs with 2060 CFCs used a value of 30 d^{-1}. These values were chosen on the basis of the relative importance of the linear and quadratic dependencies of the ozone loss rate on reactive chlorine concentration. Other than the adjustment of the k value, ozone was treated identically in all the runs performed; no attempt was made to modify the homogeneous chemical rates of change of ozone to account for different atmospheric conditions, including the H_2O change, or to impose a postulated ozone trend. Nevertheless, the ozone rate of change and distribution are sensitive to interrun differences in temperature and dynamics. More detailed chemical simulations of future ozone behaviour reveal little trend in extra-polar total ozone between 2010 and 2055 [*Austin et al.*, 2001].

4. Experimental Design

[18] The experiment performed comprised three steady-state runs differing in their complement of the radiatively active gases. Run 1995 used gas loadings from 1995 [*World Meteorological Organization* (*WMO*), 1999, Table 12.2]. This was a control simulation representing the current climate. Run 2060-A used gas loadings appropriate to the year 2060 (see below). The difference between run 2060-A and run 1995 shows the combined effect of the changes in all the radiating gases. Run 2060-B was a repeat of run 2060-A except with the CH_4 loading from run 1995. The intent of run 2060-B was to isolate the contribution of the changed CH_4, and hence H_2O, in run 2060-A compared with run 1995 to the overall difference between these two runs.

[19] All three runs used the same annually repeating SST climatology derived from observations made between 1979 and 1996. Not allowing the SSTs to change suppresses the tropospheric response somewhat, and thus has implications for wave propagation into the stratosphere. While this may affect the net stratospheric change seen between 1995 and 2060, the purpose of this work is not to forecast future climate, but to compare the response of the stratosphere to in-situ changes in H_2O with the response to changes in the other radiatively active gases. This comparison is clarified when the influence of the troposphere is reduced. Moreover, using the same SSTs means that there is little change in minimum tropopause temperature between runs, so that almost all the change in stratospheric H_2O arises from the CH_4 change, allowing this contribution to be easily isolated.

4.1. Future Gas Loadings

[20] The IPCC Special Report on Emission Scenarios (SRES) generated six marker scenarios for future trends in the radiatively active gases. Figure 2 shows the trend in tropospheric CH_4 calculated from each scenario [*IPCC*, 2001]. Each scenario is considered equally probable, but SRES B2 was chosen for this experiment because its CH_4 generally lies approximately midway between the extremes of the projections. The simulated future year, 2060, is around the last date on which the CH_4 projections remain fairly tightly grouped, thereafter their spread increases rapidly. The CO_2, CH_4, and N_2O loadings used in run 2060-A were all based on the SRES B2 emission scenario. CFC-11 and CFC-12 were taken from WMO Scenario A1 (baseline) [*WMO*, 1999]. CO_2 and the CFCs were given fixed, uniform global distributions, while for the chemically parameterized species CH_4 and N_2O the loading was applied as a fixed lower boundary condition. Because of the chemical parameterization, the H_2O difference between 1995 and 2060-A arose directly from the CH_4 difference, thus obviating the need to assume any fixed distribution for the H_2O perturbation. As explained above, ozone was treated identically in all runs save for adjusting it's rate of PSC-initiated loss to be consistent with the CFC loading. The same, unchanging, spatial distribution of aerosol was used for all runs. The loadings of the radiatively active gases used in each run are summarized in Table 1.

4.2. Integrations

4.2.1. Spin-up

[21] Runs 1995 and 2060-A were started from the same dynamic state, and spun-up for several years until the influence of gas concentrations specified at the lower boundary had propagated throughout the model domain. That is, until the parameterized species had attained a seasonally cycling approximately steady state. Run 2060-B

Table 1. Boundary Conditions for Radiatively Active Gases[a]

	O_2, ppp	CO_2, ppmv	O_3	H_2O	CH_4, ppmv	N_2O, ppmv	CFC-12, pptv	CFC-11, pptv	Aerosol
Run 1995	0.209	363.0	Cariolle	calc.	1.725	0.315	522.9	268.9	C98[b]
Run 2060-A	0.209	500.0	Cariolle	calc.	2.550	0.350	328.0	101.0	C98[b]
Run 2060-B	0.209	500.0	Cariolle	calc.	1.725	0.350	328.0	101.0	C98[b]
Band	SW	SW, LW	SW, LW	SW, LW	LW	LW	LW	LW	SW, LW

[a]O_2, CO_2, CFC-11, and CFC-12 have a uniform global distribution. CH_4 and N_2O are held constant at the lower boundary and are subject to chemistry in the middle atmosphere. H_2O in the troposphere is calculated from the model's hydrology and in the middle atmosphere is subject to chemical change. O_3 is calculated everywhere by the scheme of *Cariolle and Deque* [1986].

[b]The fixed aerosol distribution is taken from *Cusack et al.* [1998]. (The CO_2, CH_4, and N_2O loadings for 2060 differ from the SRES B2 values listed in Appendix II of *IPCC* [2001] by not more than 2%.)

was then initialized with the dynamical and chemical fields of run 2060-A, except that the CH_4 and H_2O fields were overwritten with those from run 1995. A single year's integration of 2060-B was performed to allow radiative adjustment to the new CH_4 and H_2O loadings.

4.2.2. Experiment

[22] Having thus achieved steady-state conditions for each of the runs, the experiment proper was begun, and each of the integrations was continued for a further 20 years. The twenty annual cycles so produced for each run comprise an ensemble with the same external forcings and radiative environments, but with different initial conditions. Consequently, systematic differences between runs can be distinguished from those due to internal variability.

5. Results

[23] The results are presented in two stages. First, run 2060-A is compared with run 1995; this reveals the impact on the model climate of changing all the radiatively active trace gases in line with the SRES B2 scenario, and thus simulates the net change expected between 1995 and 2060 under that scenario. Second, run 2060-A is compared with run 2060-B. This comparison reveals the individual contribution of the CH_4/H_2O difference to the net change, and hence indicates the sensitivity of climate to increased stratospheric H_2O arising from increased tropospheric CH_4. The analysis focuses on the middle atmosphere, where the radiative action of H_2O produced from CH_4 dominates the radiative action of the CH_4 itself. All results presented are ensemble means from the twenty annual cycles completed for each run.

5.1. Radiating Gases

[24] The differences between run 2060-A and run 1995 in the fixed, uniformly distributed, radiatively active gases, CO_2, CFC-11, and CFC-12 can be read directly from Table 1. Mean differences in the chemically parameterized gases O_3, N_2O, CH_4, and H_2O are shown in Figure 3 alongside their distribution in run 1995. All the fields reproduce, qualitatively and quantitatively, the main features of the current observations of the same species. Since the emphasis of the experiment is on the CH_4/H_2O system, these two species are now examined in more detail.

[25] Figure 4 compares the ensemble, mean H_2O for three separate months of run 1995 with equivalent fields constructed from version 0104 H_2O retrievals by the Microwave Limb Sounder (MLS) satellite instrument during 1991–93 [*Pumphrey*, 1999]. The difference between run 2060-A and run 1995 for these three months is also shown. (Monthly averages from individual years of the simulations and the observations show the same general features as these multiannual averages.) Morphologically, the seasonal variation in the H_2O distribution seen in the observations is well captured by the simulations except that the descent of dry air at the winter pole is more pronounced in the simulations than in the observations. This same strong descent is seen in the UM with other tracers also, indicating that it is a dynamic feature rather than an artifact of the CH_4/H_2O chemical parameterization.

[26] Quantitatively, run 1995 is markedly drier than the MLS observations throughout the middle atmosphere. The origin of this discrepancy lies in the humidity of the air entering the stratosphere from the troposphere. This is evinced by Figure 5 which shows the ensemble, annual-mean, tropical profiles of H_2O and CH_4 from the two UM runs alongside profiles from the UARS Reference Atmosphere Project (URAP) climatology. (URAP data are available from http://code916.gsfc.nasa.gov/Public/index.html.) Air in the lower stratosphere of the model is around 1 ppmv drier than the climatology. The cause is a cold bias in the tropical tropopause temperatures of the UM which results in an excess freeze drying of air ascending into the stratosphere. Inclusion of a nonorographic gwd in the UM might ameliorate this problem [*Austin et al.*, 2003]. Nevertheless, the instantaneous precipitation of all water vapor in excess of the saturation vapor pressure, as implemented in the model, is probably an oversimplification of the actual processes responsible for dehydrating air in the tropical tropopause layer. A better understanding and parameterization of these processes, and how they respond and contribute to climate change is necessary to fully characterize the total trend in stratospheric H_2O. The present work, however, examines that component of the trend due to CH_4 change alone. Notwithstanding their displacement at the tropopause, the simulated (run 1995) and observed H_2O profiles exhibit a similar stratospheric gradient, as do the CH_4 profiles, which are almost superimposed (CH_4 transport not being sensitive to tropopause temperature). The disparity between the observed and modeled H_2O in the stratosphere thus departs little from that already present when air enters from the troposphere. These facts imply that the chemical parameterization is adequately representing the true mechanism of H_2O production from CH_4 oxidation. Accordingly, the simulated response of middle-atmospheric H_2O to the change in tropospheric CH_4 between run 2060-A and run 1995 will also be correct. This response can be seen in Figure 5 with the H_2O difference between runs 1995 and

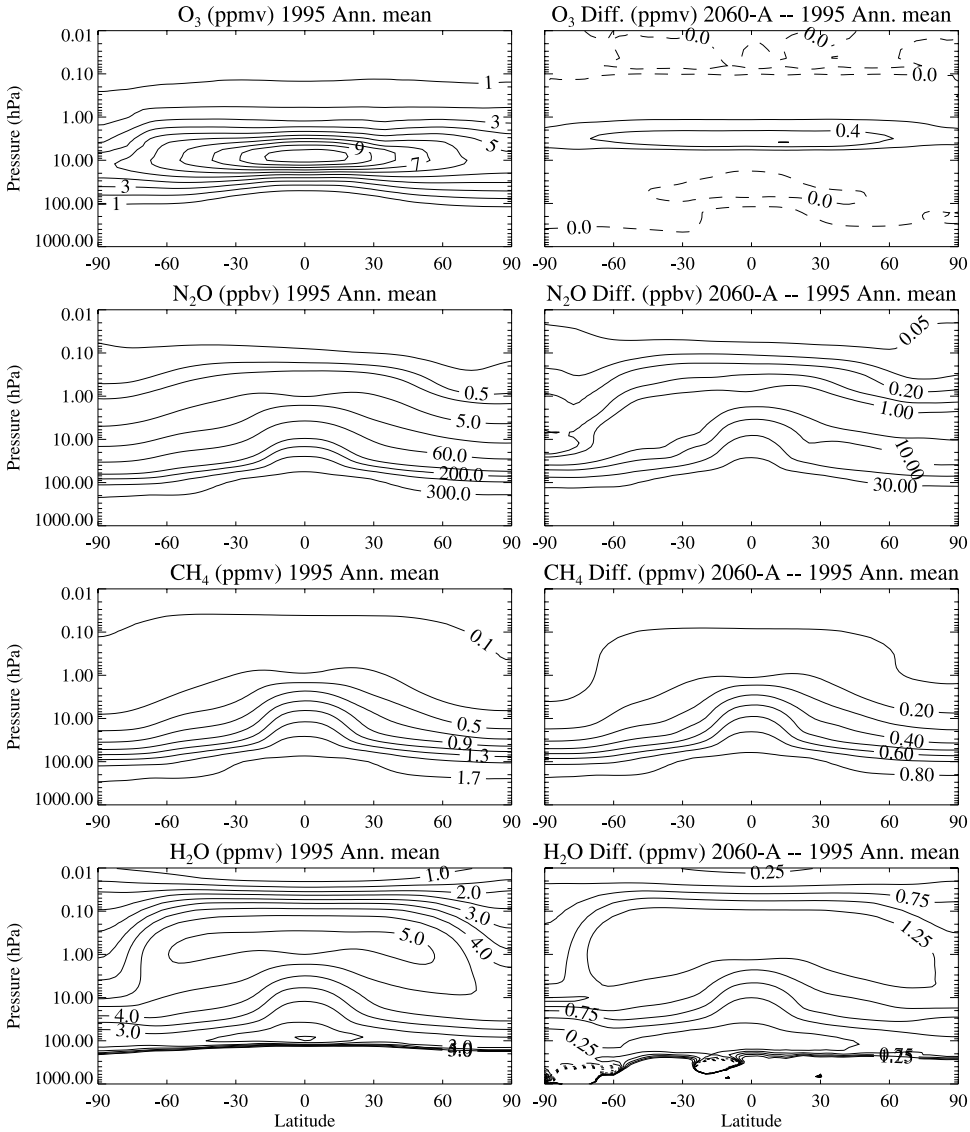

Figure 3. (left) Annual-, zonal-mean distributions of the nonuniform radiatively active gases in run 1995. (right) Differences in these gases: run 2060-A minus run 1995. All results are ensemble means, i.e., averages over the 20 annual cycles completed for each run. Positive contours are solid, and the zero contour is dashed. Note that the contour intervals for N_2O and its difference are irregular.

2060-A growing steadily from the tropopause to the stratopause as the excess CH_4 in run 2060-A is oxidized. The peak H_2O difference is ~1.5 ppmv corresponding to virtually complete CH_4 oxidation. Correctly simulating the altitude dependence of the H_2O perturbation is the chief motivation for including the chemical parameterization.

[27] A consequence of the model's background stratospheric H_2O abundance being too low is that the CH_4-derived H_2O perturbation between 1995 and 2060 although correct quantitatively is somewhat exaggerated proportionally. The radiative response to H_2O changes over this range of concentrations is, however, approximately linear [e.g., *Forster and Shine*, 2002], so the thermal and induced dynamical reaction to the H_2O change, examined below, should not be materially affected by this anomaly. The impact on the frequency of PSCs is discussed in a later section.

[28] In short, the above discussion validates the treatment of the four parameterized, radiating gases, N_2O, O_3, CH_4 and H_2O, and implies that the fields simulated for 2060 are a realistic reflection of the imposed boundary conditions.

5.2. Temperature

[29] Figure 6 presents zonal-mean, temperature differences between run 2060-A and run 1995. Results are shown for the ensemble, annual mean and for three ensemble, seasonal means. The overall pattern of the temperature difference is similar to that obtained by other model studies of the climate response to increasing greenhouse gases whether treating CO_2 alone [e.g., *Pitari et al.*, 1992; *Mahfouf et al.*, 1994] or a more complete suite of gases [*Butchart et al.*, 2000]. That is, there is a general warming of the troposphere, and a cooling of the middle atmosphere which increases with height from the tropopause up to the

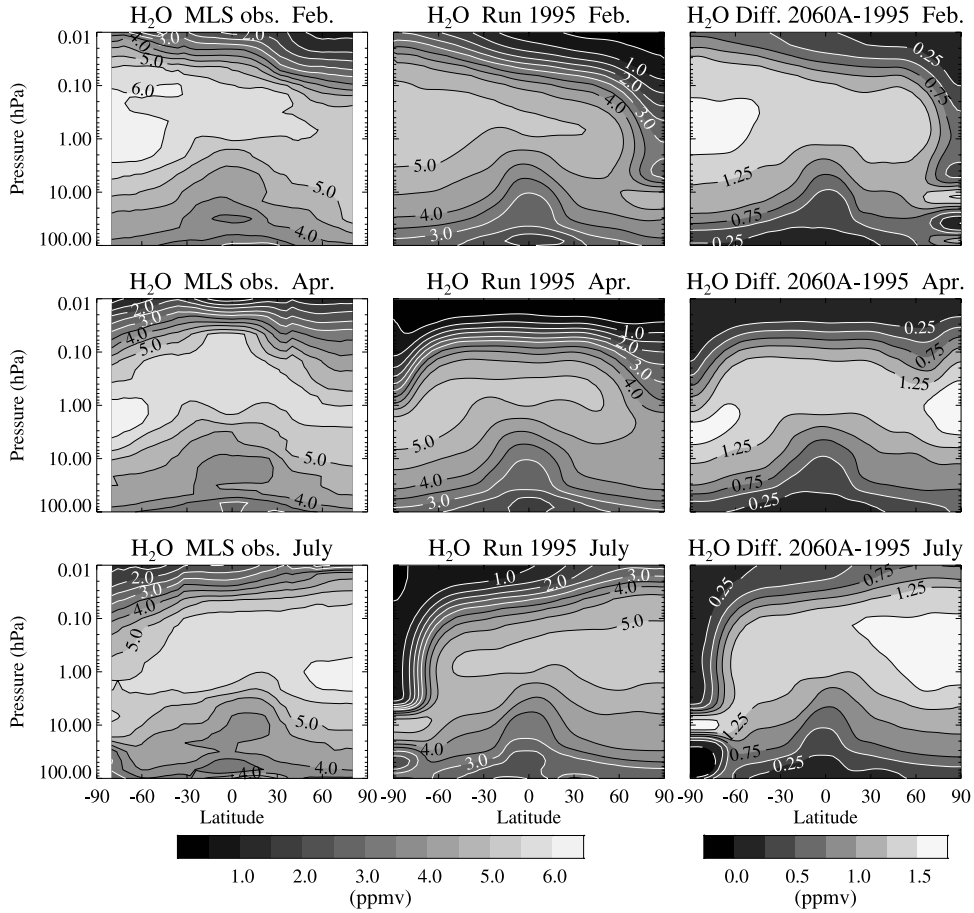

Figure 4. Monthly, zonal-mean middle-atmospheric H_2O from Microwave Limb Sounder (MLS) observations (version 0104) and from run 1995 (ensemble mean). Also shown is the difference; run 2060-A minus run 1995.

lower mesosphere. The temperature difference is seasonally variable with the relative cooling of run 2060-A peaking near the stratopause in the high latitudes of the winter hemisphere. Quantitatively, the annual-mean temperature difference of ~1 K near the tropopause rising to ~5 K at the stratopause somewhat under-represents the stratospheric trends found between 1992 and 2051 in a dynamics-only study of the UM response to projected changes in the well-mixed greenhouse gases [*Butchart et al.*, 2000]. There the temperature trend ranged from −0.16 K/decade at 46 hPa to −1.41 K/decade at 1 hPa. That study, however, used a different model configuration than is used here with different gas loadings (including a ~10% larger CO_2 trend) and included imposed trends in SST and sea-ice extent. Inclusion of a chemistry scheme with interactive ozone (though no treatment of CH_4 oxidation, or other sources of H_2O change) was found to have little effect on temperature trends in the middle stratosphere, but to reduce the cooling at 1 hPa by ~18% [*Austin et al.*, 2001]. Likewise in the present study, the relative cooling of run 2060-A is ameliorated by the response of the parameterized ozone. As the stratospheric temperature falls the photochemical tendency becomes more positive, leading to the ozone increase seen in Figure 3 and a concomitant increase in short-wave heating (~0.4 K/d in the tropical upper stratosphere) in opposition to the intensified long-wave cooling. A similar phenomenon is seen in other climate studies including fully detailed ozone chemistry [*Dvortsov and Solomon*, 2001].

[30] Having examined the impact on model temperature of changing the whole complement of radiatively active gases in accord with one possible future scenario, we now consider the individual contribution of the CH_4-derived H_2O change to that impact. This is done by comparing runs 2060-A and 2060-B, which differ only in that 2060-B has the CH_4, and hence H_2O, loading from 1995 rather than from 2060. The difference between these two runs thus reveals the contribution of the H_2O difference alone to the net change seen between 1995 and 2060-A. (Inequalities in the H_2O fields between runs 1995 and 2060-B arising from the atmospheric circulation are small in comparison to their common difference from run 2060-A.) Figure 7 shows the annual-mean temperature difference between runs 2060-A and 2060-B in absolute terms and as a percentage of the difference between runs 2060-A and 1995. Over almost all of the middle atmosphere the difference lies in the range 0.2 to 0.6 K implying that the H_2O change has contributed between 6 and 12% of the net temperature difference between the 1995 and 2060-A simulations. The fractional H_2O contribution shows a pronounced peak in the lowermost stratosphere at the poles, but the absolute temperature differences there are small. Seasonal differences (not shown) are similar to the annual mean, though less statis-

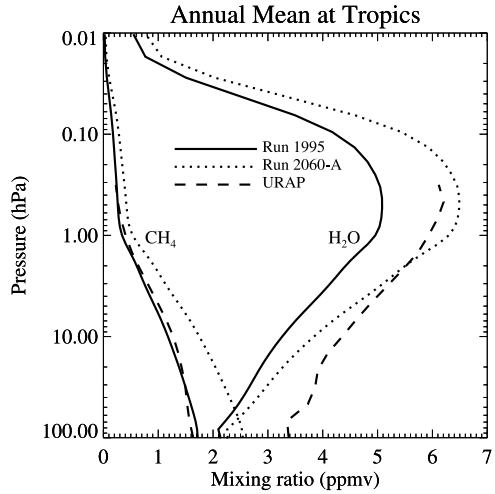

Figure 5. Annual, tropical (−16° to +16°)-mean profiles of simulated (ensemble mean) and observed H_2O and CH_4 from the runs 1995 and 2060-A and from the UARS Reference Atmosphere Project climatology. The climatology extends only to 0.3 hPa.

tically significant. The annual-mean percentage plot suggests a coherent pattern, with the H_2O difference making a relatively small contribution to the net temperature anomaly in the polar mesosphere of both hemispheres, and a larger contribution in the polar stratosphere and tropical mesosphere. The magnitudes of the temperature differences seen here are comparable to the responses of a number of radiation models to a uniform increase of 0.7 ppmv in stratospheric H_2O [*Oinas et al.*, 2001]. However, in the majority of those models, most markedly that of *Forster and Shine* [2002], the cooling is greatest in the lower stratosphere, where the radiative forcing is most sensitive to the H_2O abundance. In the present work, with the CH_4-derived H_2O perturbation growing from near zero at the tropopause to ∼1.5 ppmv at the stratopause, the cooling increases slightly with height. This vertical gradient in the response to a CH_4-derived increase in H_2O is seen also by *Shindell* [2001]. Although that study, using a model with a parameterization of the chemical effect of H_2O change on ozone, suggests a significantly larger role for H_2O from CH_4 oxidation in future cooling of the stratopause region than is seen here. Under an emission scenario comparable to SRES B2, Shindell finds that the growth in CH_4-derived H_2O from 1995 to 2060 increases the cooling at 0.7 hPa by some 4 K in excess of the cooling due to changes in greenhouse gases and ozone alone; thus contributing more than 50% of the total cooling at that height. The smaller cooling of 0.2 to 0.6 K attributed in the present work to the extra H_2O arising from the CH_4 increase between 1995 and 2060 is more commensurate with *Dvortsov and Solomon*'s [2001] result that projecting the current total stratospheric H_2O trend of +0.05 ppmv/yr in a two-dimensional model with full interactive chemistry, leads to a cooling of 0.2 to 0.3 K/decade between 2000 and 2050.

5.3. Dynamics

[31] The nonuniformity of the temperature response to a change in radiating gases implies an impact on wave-propagation and thereby on the atmospheric circulation and adiabatic heating rates. Thus the aforementioned temperature differences must arise from a combination of radiative and dynamic effects, with the radiative changes having not merely a local impact. Figure 8 shows the ensemble, annual-mean dynamic heating rates from run

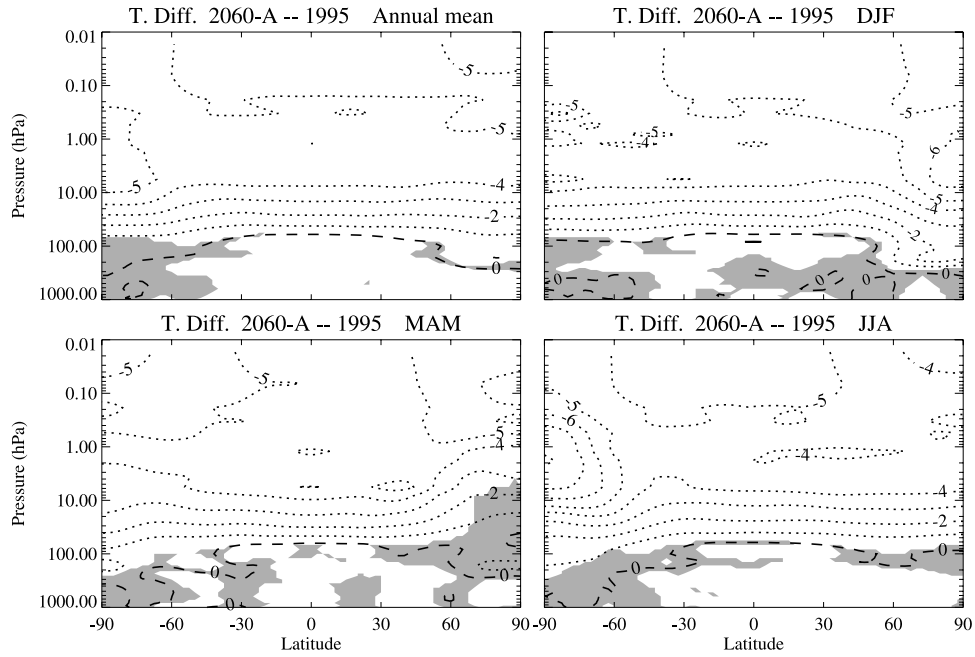

Figure 6. Ensemble, annual and seasonal, zonal-mean temperature differences: run 2060-A minus run 1995. The seasons shown are December/January/February, March/April/May, and June/July/August. The shading indicates where the significance of the difference is less than 0.95 in a Student's t test. The contour interval is 1 K. Negative contours are dotted, and the zero contour is dashed.

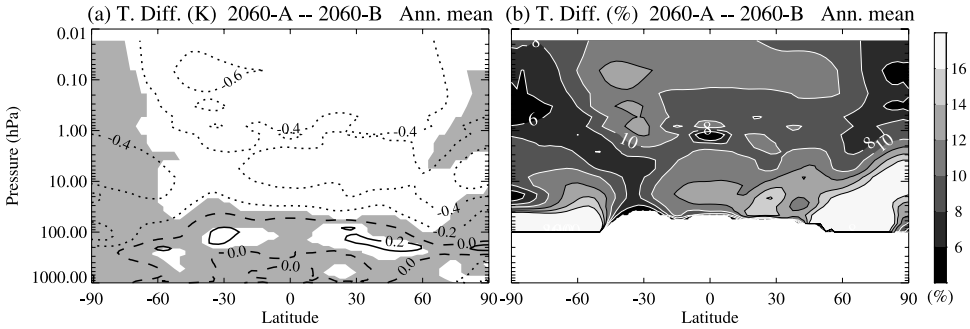

Figure 7. Ensemble, annual, zonal-mean temperature difference: run 2060-A minus run 2060-B. (a) Absolute difference. The contour interval is 0.2 K. Negative contours are dotted, and the zero contour is dashed. The shading indicates where the significance of the difference is less than 0.95 in a Student's t test. (b) Difference as a percentage of the difference between runs 2060-A and 1995 (the troposphere is omitted).

2060-A, and their differences from those from runs 1995 and 2060-B. These heating rates, inferred from the inequality between the radiative heating rates and the temperature tendency, are, effectively, a product of the vertical residual circulation in the transformed Eulerian mean perspective.

[32] The adjustment in the heating rates between runs 1995 and 2060-A shows a symmetrical distribution strongly suggestive of a systematic impact on the model's middle-atmospheric circulation. Moreover, the sign and magnitude of the difference correlates closely with the sign and magnitude of the heating rate itself. That is, where there is ascent (adiabatic cooling) the difference is positive, and where there is descent (adiabatic warming) the difference is negative. In other words, the general circulation of run 2060-A is strengthened compared with that in run 1995. The only exception is in the southern polar stratosphere, where the descent rate is somewhat reduced. This intensification of the residual circulation and global dynamic heating rate is similar to that found in the doubled CO_2 experiment of *Rind et al.* [1998], where it is attributed to increased wave forcing of the zonal flow. The consequence of the circulation response is that the excess radiative cooling arising from the changed gas loading in 2060 is amplified in tropical latitudes and, for the most part, reduced at higher latitudes. A semblance of the same pattern can be seen in the dynamic response to a change in H_2O alone, as indicated by the 2060-A versus 2060-B difference plot. The outstanding feature of that plot, however, is the relatively large contribution of the H_2O change to the increased heating near the northern polar stratopause. In both hemispheres the maximum heating rate is around 5 to 7% greater in 2060-A than in 1995, but whereas the contribution of the H_2O change to the difference in the south is small, in the north the H_2O change accounts for around half of the net increase. This despite there being little hemispherical asymmetry in the H_2O change itself (see Figure 3). Although the peak 2060-A versus 1995 and 2060-B heating-rate differences occur at the poles where the large dynamic variability reduces the statistical significance below 95%, the region of greater significance is sufficiently extensive to well-define the coherent global pattern of the differences including the hemispherical asymmetry. Moreover, even where not statistically established, the polar differences are consistent with the general pattern. There is thus a suggestion that for the chosen future scenario the Northern Hemisphere circulation is more sensitive to an H_2O increase than is the Southern Hemisphere.

[33] To investigate this further, the high-latitude temperatures and dynamic heating rates and their interrun differences are expanded in Figure 9 from their annual means into their mean annual cycles. These seasonal results are not quantitatively robust, but they do afford a qualitative insight into the ongoing processes. At both poles, the annual means of the 2060-A versus 1995 differences in temperature and heating rates are dominated by events during late winter and spring, when dynamic activity is greatest. Throughout this time the dynamic response triggered by the change in the radiative environment overwhelms the initial radiative signal, as is evinced by the occurrence of both positive and negative anomalies in LWHR (not shown), modulated by the temperature difference. This applies in both hemispheres although the evolutions of the difference fields in the north are somewhat more complex than in the south, and show a stronger downward propagation. The contribution of the increased H_2O in 2060 to the overall response is given by the difference between runs 2060-A and 2060-B. In the north the 2060-A versus 2060-B differences in temperature and in the heating rates clearly share, albeit at reduced intensity, the characteristics of the 2060-A versus 1995 differences. In the south, by contrast, the 2060-A versus 2060-B differences are small, and have little obvious structure. The seasonally evolving results thus support the inference drawn from the annual means that the H_2O component of the change in radiative environment between 1995 and 2060 is having a larger relative impact on the northern hemispheric circulation than on the southern.

5.3.1. Wave Propagation

[34] The middle-atmospheric circulation is ultimately controlled by waves upwelling from the troposphere [*Haynes et al.*, 1991]. Changes in the wave driving might arise from a change in the intensity of tropospheric wave generation and/or a change in the propagation and dissipation of the waves aloft. The eddy heat flux (EHF) is used to compare these processes in the different runs, concentrating on winter when the largest interrun differences arise. Figure 10 shows the ensemble, seasonal-mean profiles of EHF at 60° latitude for the two hemispheres; the values at 100 hPa may be taken to represent the tropospheric planetary-wave energy entering

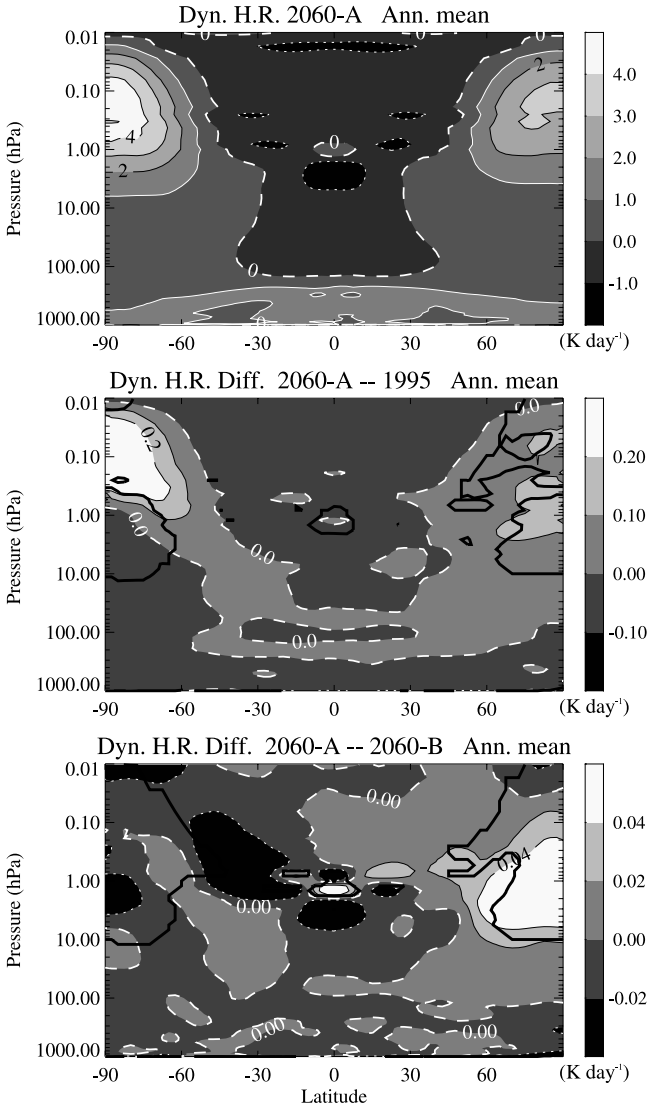

Figure 8. Ensemble, annual, zonal-mean dynamic heating rate from run 2060-A and the differences: run 2060-A minus run 1995 and run 2060-A minus run 2060-B. The difference fields are smoothed with a three-by-three-point (altitude/latitude) moving average. Note that the contour scale differs for each panel. Negative contours are dotted, and the zero contour is thickly dashed. The thick black line on the difference plots is the contour of 95% statistical significance (indicating areas below this significance at the high latitudes).

the stratosphere [*Newman et al.*, 2001]. An increase in upwelling tropospheric energy has been reported as a symptom of climate change in a number of previous studies with the UM [*Butchart et al.*, 2000] and other models [*Rind et al.*, 1990, 1998]. Here, though, there are no statistically significant interrun differences in the 100 hPa EHF, probably as a consequence of the runs all using the same SSTs. Thus changes in the planetary-scale tropospheric forcing do not appear to explain the circulation changes occurring between runs. On ascending the stratosphere, however, there do develop increasingly significant interrun differences in the EHF, suggesting inequalities in the vertical wave propagation. Strikingly, in the northern, upper stratosphere, the EHF inequality between runs 2060-B and 2060-A becomes larger than that between runs 2060-A and 1995, and is significant at greater than the 95% confidence level. This implies that the H_2O increase between 1995 and 2060 is having a large impact on the vertical gradient of EHF, and hence on the vertical wave propagation. The growth from the mid to the upper stratosphere of the fractional EHF change attributed to the H_2O resembles the distribution of the H_2O perturbation itself. Although it is difficult to establish a robust quantitative relationship between the impact of the H_2O change on the strength of the wave forcing and on the dynamic heating rates, they both being highly variable quantities, this modulation of the planetary-wave propagation, which causes a greater deceleration of the mean, zonal flow as indicated by the E-P flux divergence (not shown) is the likely explanation for the large contribution of the H_2O increase to the change in northern hemispheric circulation between 1995 and 2060.

[35] In southern winter, by contrast, the growth of EHF with height is less in the 2060 runs than in 1995, indicating a reduced vertical wave propagation. Also, the relative contribution of the extra H_2O in 2060 to the difference is smaller. A reduced planetary-wave forcing of the circulation is in agreement with the smaller dynamic heating rates noted earlier in the Southern Hemisphere stratosphere of 2060. In the mesosphere where the dynamic heating rate is greater in 2060, the flow will be controlled mainly by breaking gravity waves. The opposite effects of the change in radiative environment on the planetary-wave propagation and stratospheric circulation in the different hemispheres may be associated with the impact on the latitudinal temperature gradient in the lower stratosphere. The cooling just above the tropopause in 2060 varies little with latitude, but the predominant sign of the change in the pole to equator temperature gradient will determine whether the middle-latitude zonal flow is generally increased or decreased, with ensuing consequences for the propagation and refraction of upwelling waves. Although the mechanism is subtle, the fact that the net 2060 versus 1995 differences in dynamic heating rate are statistically significant in the stratosphere of both hemispheres, but of opposite sign, suggests a systematic interhemispheric difference in the dynamic responses.

5.3.2. Sudden Stratospheric Warmings

[36] In addition to the impact on the mean circulation, the effect of climate change on the occurrence of sudden stratospheric warmings (SSWs) is also of import, particularly in the Arctic where changes in the frequency of such events appear key to determining future ozone depletion [*Austin and Butchart*, 1994]. Over the 20 years of integration, run 2060-A has ~50% fewer Arctic warmings, defined as a reversal of the pole to 60° zonal-mean temperature gradient at 10 hPa, than run 1995 (8 as opposed to 17). In run 2060-B where the contribution of the extra H_2O is removed, the number of SSWs (16) is almost the same as in run 1995. Although seemingly further evidence for the importance of H_2O change to the northern dynamics, this asymmetric distribution of warmings between runs is not significant in a chi-square test, and may be due simply to internal variability [*Butchart et al.*, 2000]. The results do, though, support findings from other model simulations that

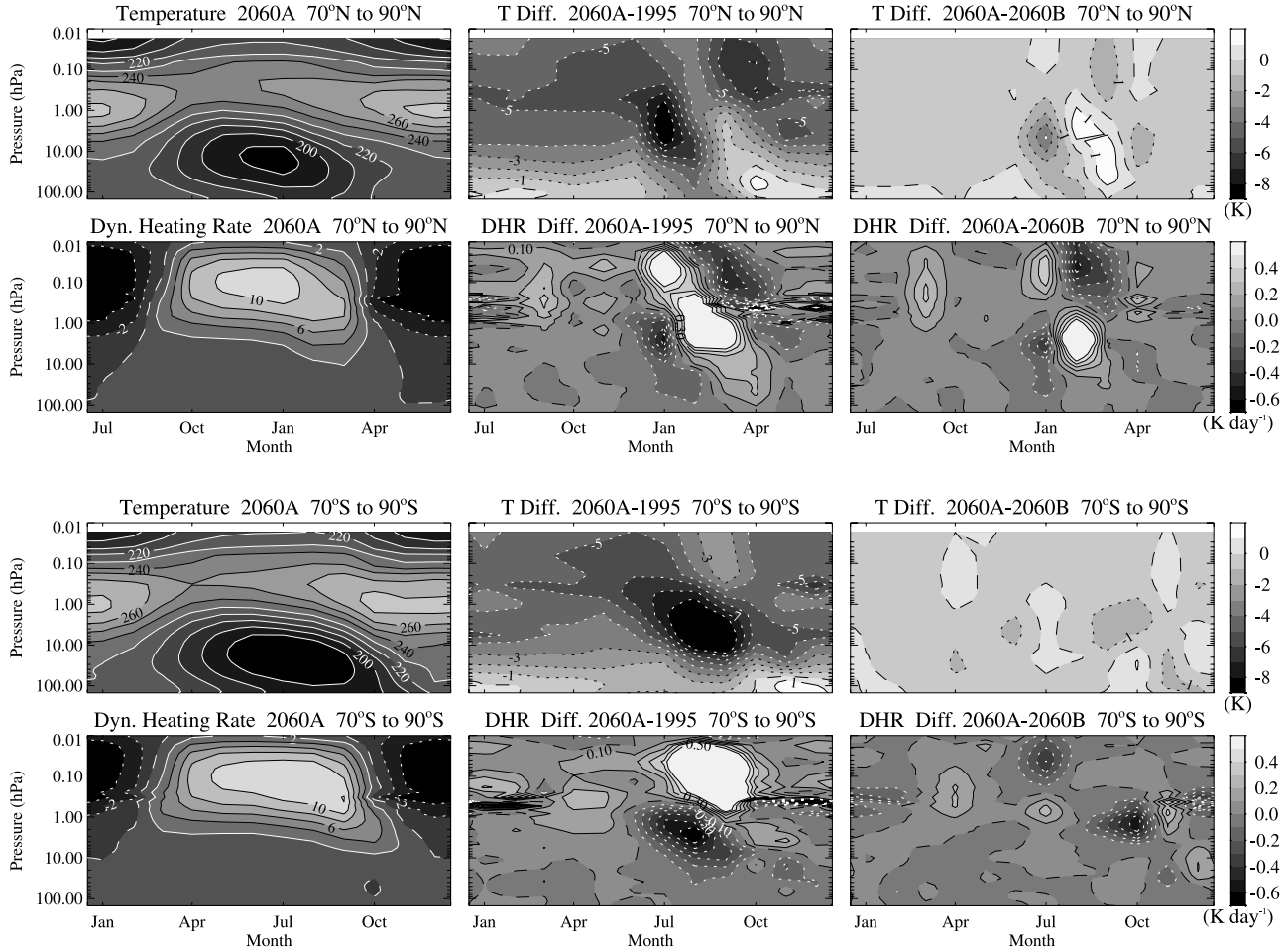

Figure 9. Ensemble, mean annual cycles of temperature and dynamic heating rate from run 2060-A, and the differences run 2060-A minus run 1995 and run 2060-A minus run 2060-B. The topmost six plots show the average from 70°N to 90°N, and the bottom plots show the average from 70°S to 90°S. Note that for the northern plots the time axis is offset by six months. The color bars apply to the difference plots. Negative contours are dotted, and the zero contour is dashed.

a strengthened wave forcing and Arctic circulation can coexist with a reduced frequency of SSWs over a multidecadal period [e.g., *Shindell et al.*, 1998].

5.3.3. Vortex Climatology

[37] The climatologies of the polar vortices in the various runs are compared using elliptical diagnostics [*Waugh*, 1997]. This method enables construction of a single ellipse representing the mean state of the polar vortex over an arbitrary averaging period. February-mean results from runs 1995, 2060-A, and 2060-B for the Arctic vortex on the 700 K isentrope are shown in Figure 11. The aspect ratio, position, and orientation of the vortex are similar in all three runs, suggesting that the increase in greenhouse gas loadings between 1995 and 2060 has caused no major change to the general polar flow regime. Nevertheless, the vortex is slightly larger in the 2060 runs, which is consistent with their lower temperatures provoking an intensification of the existing circulation. The vortices from runs 2060-A and 2060-B are very alike in all regards, including size, which indicates that, notwithstanding the large impact of the extra H_2O in 2060-A on the dynamic heating rate, the mean vortex morphology remains largely unaffected by the H_2O increase. In the south (not shown), the monthly mean vortices from the three runs are almost indistinguishable.

5.4. Age of Air

[38] The age of air, i.e., the time elapsed since air in the middle atmosphere last left the troposphere is a convenient way of quantifying changes in the general circulation. This quantity was evaluated using the age-spectrum approach [*Hall and Plumb*, 1994], where the distribution of ages within a given air parcel is calculated by following the evolution of a passive tracer with a pulsed source in the tropical troposphere. Figure 12a shows the mean age of air from run 2060-A. The age field with its vertical gradient increasing sharply with latitude, and the oldest air located in the polar stratosphere, resembles that derived from previous studies with other models. Figure 12b demonstrates that the air throughout most of the middle atmosphere is younger in run 2060-A than in run 1995, supporting the implication of the dynamic heating rates that the air is circulating faster in 2060. Albeit the age differences are relatively small, peaking, near the northern pole, at ~0.3 years compared with a maximum age in excess of ~5.5 years. Figures 12c and 12d

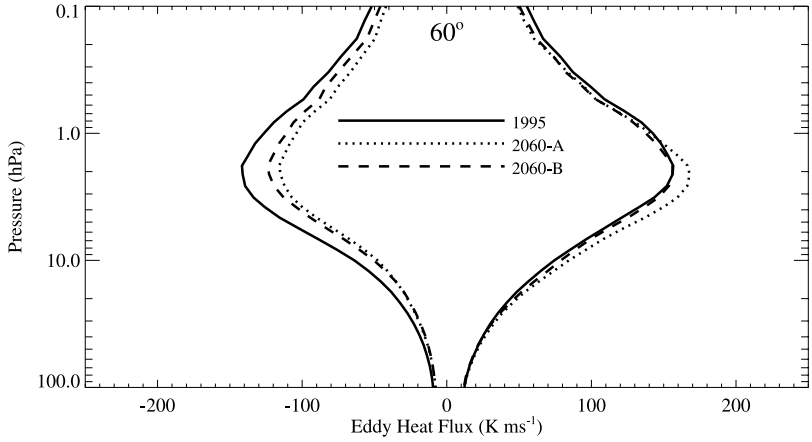

Figure 10. Ensemble, mean eddy heat fluxes from runs 1995, 2060-A, and 2060-B at 60° latitude for northern winter (DJF) and southern winter (JJA). Negative values are for the south.

show the age differences (run 2060-A versus run 2060-B, and run 2060-B versus run 1995), thus revealing the contributions of the H_2O and non-H_2O perturbations, respectively, to the net change in mean age between 1995 and 2060. The two contributions are clearly distinct. Whereas the non-H_2O perturbation lowers the mean age throughout the middle atmosphere, the H_2O perturbation lowers the mean age in the mesosphere, but increases it in the stratosphere. In addition, the H_2O change alone accounts for virtually all the hemispherical asymmetry in the overall response, causing a markedly greater diminution of mean age in the Arctic latitudes, where the H_2O-derived diminution extends down into the stratosphere and peaks at ~0.2 years, than in the Antarctic. The response of the age is therefore consistent with the response of the dynamic heating rates in suggesting that the H_2O change affects the northern circulation more than the southern. Furthermore, the age response strongly suggests that the spatially varied H_2O increase in 2060 impacts the general circulation in a systematically different way than does the uniform CO_2 increase responsible for the bulk of the residual response. Whether this is a consequence of the morphology of the H_2O perturbation, or of the different radiative properties of the two gases, or of a combination of both is not clear. Nonetheless, this dynamic disparity must be at least partially responsible for the differently distributed temperature changes wrought by the H_2O-only and by the net radiative perturbations between 1995 and 2060.

5.5. Age/N_2O Correlation

[39] A change in the middle-atmospheric circulation must impact the distribution of any long-lived, but reactive, chemical species. Particularly one such as N_2O whose mixing ratio in a given air parcel depends almost exclusively on the total past exposure of that parcel to ultraviolet (UV) radiation. The correlation between age and N_2O is examined in Figure 13, which has the ensemble, annual, zonal-mean N_2O at each latitude/pressure grid point plotted against the mean age of air. Run 2060-A is compared against both run 1995 and run 2060-B (with the N_2O from the run 1995 scaled to account for its smaller lower boundary condition in that year). For all runs, the spread of N_2O values found in air of a given age increases as the age increases. This is symptomatic of equally aged air parcels having followed different trajectories within the middle atmosphere, and hence having had different exposure to UV radiation. It can be seen from Figures 13a and 13b that initially the distributions from runs 1995 and 2060-A are similar, but as the air ages there is, both in the north and in the south, a separation into two distinct groupings as the curve from 2060-A steepens more sharply than that from 1995. This steepening is consistent with an intensified circulation in 2060-A, meaning that air of a given age has on average ascended higher in the atmosphere and has thus experienced a greater UV insolation. It is noticeable, though, that in 2060-A the spread of N_2O values converges again to relatively high values in the oldest air. This old air is located in the lowermost stratosphere of the high lat-

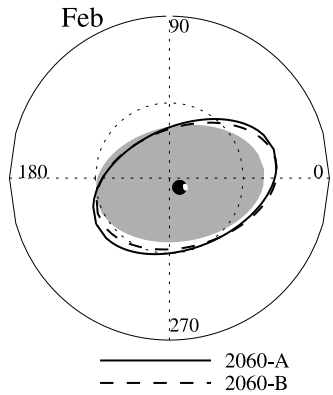

Figure 11. Polar stereographic maps of the ensemble, February-mean equivalent ellipses on the 700 K isentrope for the Arctic vortices of runs 1995, 2060-A and 2060-B. The ellipse for 1995 is shown in grey shading, and the perimeters of the 2060-A and 2060-B ellipses are indicated by solid and dashed lines, respectively. The edge of the maps is at 30°N, and the dotted inner circle is at 60°N. In calculating the equivalent ellipses the vortex edge was defined by the 2.0×10^{-4} K m^2 kg^{-1} s^{-1} potential vorticity contour. The centroid of the 1995 ellipse is marked by a black disc, and the centroids of the 2060-A and 2060-B ellipses by (barely resolved) smaller white discs.

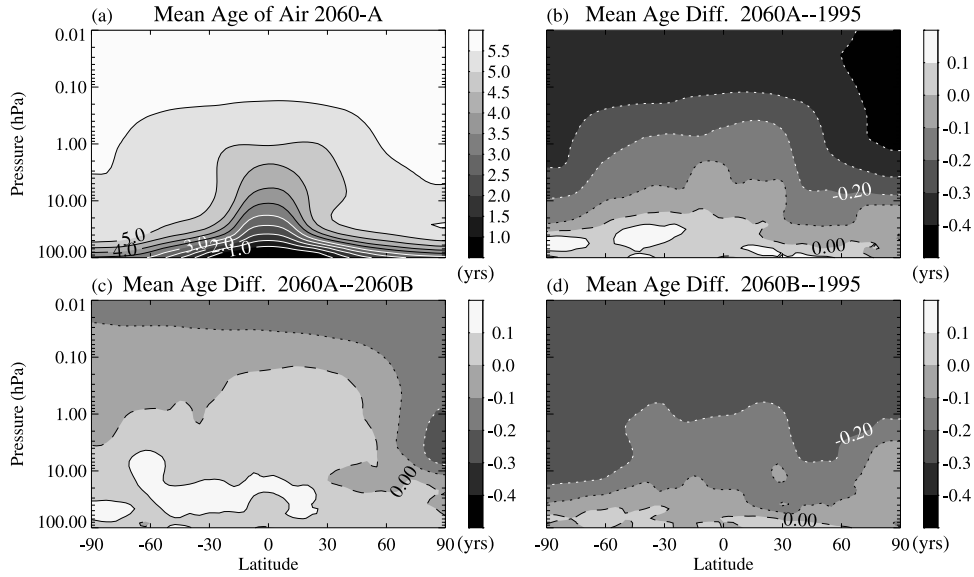

Figure 12. (a) Mean age of middle atmospheric air in run 2060-A (i.e., the mean transit time from the troposphere of all the particles comprising a given air parcel). (b, c, and d) Differences in age: run 2060-A minus run 1995, run 2060-A minus run 2060-B, and run 2060-B minus run 1995. Negative contours are dotted, and the zero contour is dashed.

itudes, and the implication is that it has traveled there from the tropics along a low-altitude trajectory with small meridional velocity. In run 1995 the oldest air has the lowest N_2O loading, another indication of a circulation change between the 2 years. Comparison of the two hemispheres reveals that in run 1995 the spread of ages in the most N_2O-poor air is less compact in the north than in the south, but that in run 2060-A the northern spread has tightened to resemble that in the south.

[40] The individual contribution of the H_2O change to the 2060 versus 1995 difference is illustrated in Figures 13c and 13d, which juxtapose the results from run 2060-A with those from run 2060-B. In the south, the two distributions are little different indicating a small role for H_2O. In the

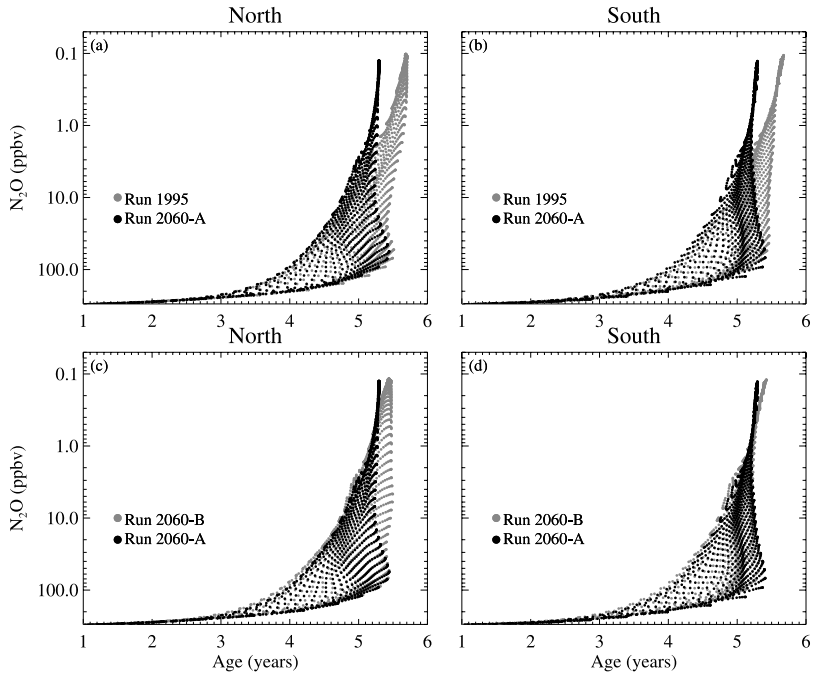

Figure 13. Mean age of air versus ensemble, annual, zonal-mean N_2O mixing ratio. Each filled circle represents one latitude/level grid point. (a) Comparison of run 1995 and run 2060-A in the Northern Hemisphere; (b) run 1995 and run 2060-A in the Southern Hemisphere; (c) run 2060-B and run 2060-A in the Northern Hemisphere; (d) run 2060-B and run 2060-A in the Southern Hemisphere.

north, however, the tightening of the low-N_2O age distribution noted in run 2060-A with respect to run 1995 is largely absent from run 2060-B, implying that the main cause of the tightening is the increased H_2O in 2060. Again this is evidence of the H_2O change having a larger impact on the Northern Hemisphere circulation than on the Southern Hemisphere, and the suggestion from the age/N_2O correlation is that the effect of the H_2O is to make the circulation in the north, in some regard, more similar to that in the south.

5.6. Polar Ozone Loss

[41] A major concern regarding future climate change is the implication for wintertime polar ozone loss. Cooling of the stratosphere due to increased greenhouse gas loading might promote the formation of PSCs, leading to a greater release of active chlorine, and thus to a greater ozone loss [*Austin et al.*, 1992; *Shindell et al.*, 1998]. Water vapor change plays a unique part in this process because H_2O, being itself a constituent of PSCs, can influence the cloud frequency not only by changing the atmospheric temperature, but also by changing the temperature at which the clouds can form. All else being equal, the higher the H_2O abundance, the higher the threshold temperature for PSCs and the greater their prevalence. The net change in PSC frequency between 1995 and 2060, and the resulting consequences for ozone loss, are examined below, emphasizing the role of H_2O. As already discussed, the stratospheric H_2O in the 1995 simulation has a low bias of around 1 ppmv compared with observations of the same year. Consequently, there will be a corresponding low bias of around 3 K in the simulated threshold temperature for PSC formation (assuming a lower stratospheric humidity of 3 ppmv instead of 4 ppmv); this will lead to some reduction in the 1995 PSC frequency. Furthermore, the sensitivity of the threshold temperature to H_2O concentration is approximately 20% greater at the lower humidity, meaning that the growth in PSC frequency found between 1995 and 2060 will be increased accordingly. Nevertheless, these small biases notwithstanding, the attribution of the interrun differences in PSC occurrence and their ensuing impact on polar ozone, helps illuminate the relative susceptibilities to different aspects of climate change.

[42] Water vapor, temperature, PSC area, chlorine activation index (Cl_i), and ozone fields from the Arctic and Antarctic vortices of run 1995 are shown in Figure 14 along with their differences from the corresponding fields of run 2060-A. Results are presented for the lower stratosphere as a function of time and potential temperature. Note that whereas the PSC distribution is inferred from the model's temperature and H_2O fields in a fairly rigorous manner (albeit assuming fixed HNO_3 and H_2SO_4 abundances), the ensuing inference of Cl_i and ozone-destruction rate is highly simplified. As expected, the elevated H_2O and decreased temperature in 2060-A combine to increase the area occupied by PSCs. The magnitude of the 2060-A excess is similar in the two hemispheres, but the relative change is larger in the north, where the time-integrated increase in cloud area ranges from $\sim$300% at 420 K to $\sim$100% at 500 K and above. The relative increase in the south shows the opposite trend with height but peaks at around 45%. Enhanced formation of PSCs near the year 2060 has also been reported by *Butchart et al.* [2000] and *Austin et al.* [2001], although those studies used a different PSC measure, hindering a quantitative comparison. In both hemispheres, the PSC increase is accompanied by a rise in Cl_i. In the Antarctic, where the chlorine in midwinter is nearly fully activated even in 1995, the rise manifests mainly in the early winter and in the spring.

[43] The effect of chlorine-catalyzed ozone destruction is apparent in both hemispheres of 1995, where the ozone mixing ratio in the lower stratosphere either stabilizes (Arctic) or declines (Antarctic) at a time when the dynamic tendency is positive. Nevertheless, notwithstanding the greater activation of the available chlorine, the vortex ozone amount in 2060-A is always greater than in 1995, by up to $\sim$0.7 ppmv in the north and $\sim$1.0 ppmv in the south. This indicates that, with the applied scaling of the ozone loss rate according to CFC loading, the decrease in total chlorine in 2060 outweighs its increased activation, in agreement with previous studies [*Shindell et al.*, 1998; *Austin et al.*, 2001; *Rosenfield et al.*, 2002]. Intensified solar heating arising from the reduced ozone loss in 2060-A is the probable cause of a faster springtime rise of temperatures in that run, which eventually reverses the sign of the temperature anomaly in the lower stratosphere of both vortices. Consequently, the PSC lifetime is not significantly prolonged in 2060-A relative to 1995. Within each individual winter there will be a complex interaction between H_2O, temperature, PSC amount, Cl_i, and ozone inside the polar vortex. This ozone modulated radiative-chemical feedback is discussed more fully by *MacKenzie et al.* [1999] and *MacKenzie and Harwood* [2000].

5.6.1. Role of H_2O

[44] Having looked at the general pattern of the 2060 versus 1995 difference, we now focus on the role of H_2O in creating that difference. Figures 15a and 15b show the gaseous H_2O difference between run 1995 and run 2060-A on the 465 K isentrope (i.e., taking a horizontal section through Figure 14). This level is the approximate location of maximum chlorine activation and ozone destruction. In both hemispheres, descent of air which has undergone more complete CH_4 oxidation causes the interrun H_2O difference to grow steadily until shortly after midwinter. Thereafter the difference in the north dips somewhat and then stabilizes while the difference in the south decays continuously, so that for the remainder of the southern winter and spring the H_2O abundances in 1995 and 2060 are almost equal. The hemispheric asymmetry is explained by the lower temperatures of the southern vortex. An abrupt diminution in gaseous Antarctic H_2O which occurs in run 2060-A, and nearly simultaneously, but less markedly in run 1995, is initiated by the temperature falling to the point at which the atmospheric water vapor becomes saturated with respect to ice. The H_2O then adjusts rapidly to the saturated mixing ratio. Thus while the temperature remains sufficiently low, it alone governs the abundance of gaseous H_2O in the Antarctic vortex, and there is no sensitivity to the different CH_4/H_2O loadings in runs 1995 and 2060-A. The interrun differences in saturated vortex H_2O that arise because of temperature inequalities are small relative to the unsaturated H_2O differences. Moreover, removal of the excess, frozen, H_2O by sedimentation means that there is no immediate restoration

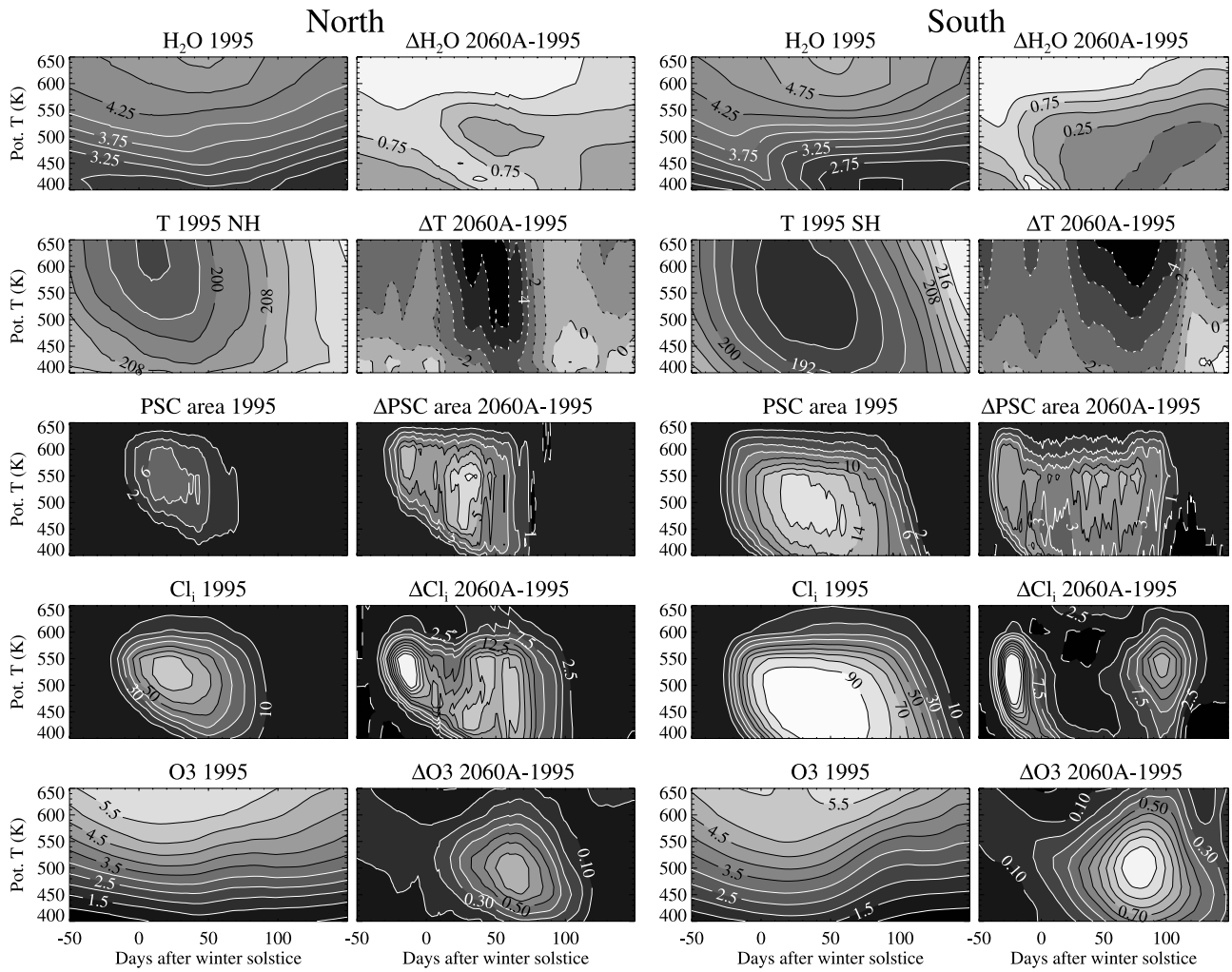

Figure 14. Winter and spring evolution of vortex-averaged H_2O, temperature, PSC area (not vortex-averaged), chlorine-activation index, and ozone from run 1995, and the differences run 2060-A minus run 1995. These are ensemble means from each run. The contour intervals are 0.25 ppmv, 4 K, 2×10^{12} m^2, 10%, and 0.5 ppmv for the fields, and 0.25 ppmv, 1 K, 1×10^{12} m^2, 2.5%, and 0.1 ppmv for the differences. Lighter shading indicates larger (more positive) values. Negative contours are dotted, and the zero contour is dashed. The vortex boundary was taken as the 65° equivalent latitude contour as calculated from the potential vorticity. Results are shown for both Northern (NH) and Southern (SH) Hemispheres.

of the Antarctic H_2O difference when the sub-saturation temperatures dissipate. A moderate formation of ice within the northern vortex of run 2060-A causes the aforementioned dip in the H_2O excess relative to run 1995, but a substantial difference between runs persists throughout the northern winter.

[45] As mentioned earlier, an H_2O difference can impinge on the PSC frequency in two ways: by altering the vortex temperature; and microphysically by altering the temperature at which PSCs are thermodynamically possible. The first mode of action can not be reliably quantified from the present experiment because the individual impact of the H_2O on the evolving temperature of the lower vortex is not statistically well established. The second mode can, however, be quantified, and compared with the effect of the net temperature change between 2060 and 1995, shown in Figures 15c and 15d. To this end, the PSC area has been recalculated off-line using the temperature from run 2060-A in conjunction with the H_2O from run 1995. This subtracts the PSC response due to the microphysical effect of the extra H_2O in 2060, and isolates the response due to the temperature change alone. The results at 465 K are shown in Figures 15e and 15f. The area under the solid line represents the net PSC increase between 2060 and 1995, while the area under the dotted line represents the increase remaining after removing the microphysical effect of the extra H_2O. In the north the extra H_2O accounts for some 26% of the net growth in time-integrated PSC area between 1995 and 2060, and in the south ~18%. These proportions vary little with height, except that the H_2O makes a somewhat larger contribution in the very lowermost stratosphere. Although the interyear H_2O difference is generally smaller in the south than in the north, this is partially compensated by the increased

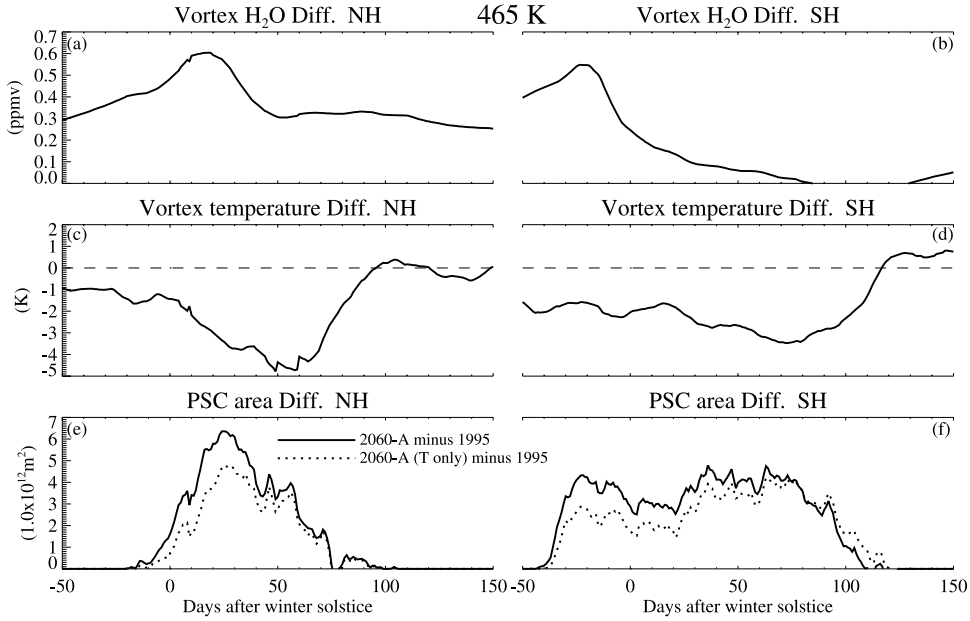

Figure 15. Difference in (a and b) vortex-averaged gaseous H_2O, (c and d) vortex-averaged temperature, and (e and f) PSC area at 465 K between run 1995 and run 2060-A (run 2060-A minus run 1995). The PSC panel also shows the difference between the PSC area from run 1995 and the area calculated using the H_2O from run 1995 and the temperature from run 2060-A, this latter difference being labeled 2060-A (T only) minus 1995. These are ensemble means from each run. Results are shown for both Northern (NH) and Southern (SH) Hemispheres. The vortex boundary is the same as in Figure 14.

sensitivity of the PSC threshold temperature to H_2O mixing ratio at the lower temperatures of the southern vortex. Thus the microphysical effect of the CH_4-derived H_2O excess makes a significant contribution, relative to the contribution of the net climatic cooling, to the total PSC increase in both vortices.

5.6.2. Implications for Ozone

[46] Figure 16 shows the evolution of vortex ozone attributable solely to PSC-initiated chemistry from each of the three runs. Other chemical and dynamical influences have been removed by subtracting the field of a second ozone tracer not susceptible to the parameterized PSC chemistry. As explained above, the ozone destruction in 2060 is less than in 1995 owing to the reduced total chlorine. This negative impact overwhelms the positive impact of the increased fractional chlorine activation in 2060, which consequently cannot be quantified. However, because runs 2060-A and 2060-B both used the 2060 chlorine loading but used CH_4/H_2O loadings from 2060 and 1995 respectively, the difference in their ozone evolutions corresponds to the extra destruction in 2060 due to the increased H_2O. In the Antarctic vortex, the H_2O effect on the ozone loss is negligible because for the bulk of the winter, when the majority of the ozone loss takes place, the chlorine activation is not limited by the PSC amount. In the Arctic, however, the chlorine activation is not so complete, and the relatively large increase in PSC area between 1995 and 2060 stemming from the rise in H_2O causes a perceptible enhancement of Cl_i and hence of ozone destruction. Although this enhanced destruction is small in absolute terms, it represents an approximate 15% increase in the peak loss. Moreover, this fractional H_2O contribution will likely be near constant with chlorine loading, so should this loading not dwindle as forecast, then a future CH_4/H_2O increase might be responsible for a substantial, in absolute terms, enhancement of ozone loss within the Arctic vortex. The H_2O contribution in the

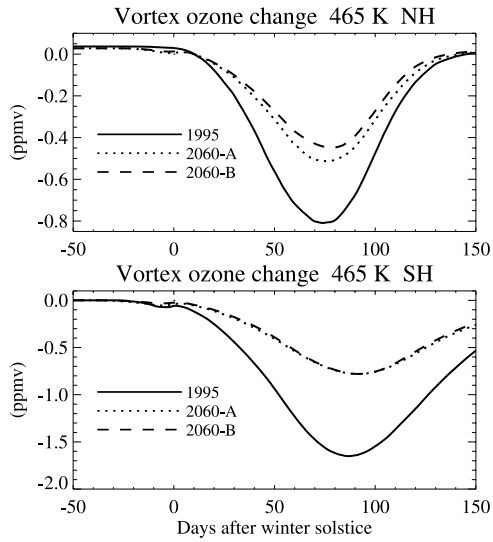

Figure 16. Vortex-averaged ozone change (due to PSC-initiated chemistry only; see text) on the 465 K isentrope from runs 1995, 2060-A, and 2060-B (the last two are almost coincident in the south). These are ensemble means from each run. Results are shown for both Northern (NH) and Southern (SH) Hemispheres. Note the different scaling of the *y* axis on the two panels. The vortex boundary is the same as in Figure 14.

Antarctic, by contrast, will be always small, whatever the chlorine loading.

6. Summary and Conclusions

[47] The inclusion of a simple chemical parameterization in the Met Office Unified (general circulation) Model has enabled generation of a realistic response of middle-atmospheric H_2O to an imposed change in tropospheric CH_4. The spatial distribution of the H_2O perturbation evolves naturally from and consistently with the model's dynamics and chemistry, obviating the need for any assumptions regarding this radiatively important aspect of the response.

[48] Under the IPCC SRES-B2 emission scenario, the cooling of the 2060 middle atmosphere relative to that in 1995 peaks in the upper stratosphere and mesosphere at around 5 K, with the CH_4-derived increase in H_2O accounting for ~10% of the change. The decreased temperature in 2060 is accompanied by a general strengthening of the global circulation, although the average descent rates in the southern stratosphere are reduced. This strengthening reduces the mean age of middle-atmospheric air and impacts the dynamic heating rates, intensifying the cooling effect of the altered radiative environment in the tropics and opposing it at the poles. Seen in isolation, the component of the circulation change attributable directly to the H_2O increase is not simply a weaker analogue of the overall response, but it has, instead, somewhat different qualitative properties. Whereas the overall dynamic response is hemispherically symmetrical, and gives younger air throughout the middle atmosphere, the individual H_2O response causes a markedly greater increase in the descent rate in the northern high latitudes than in the southern, and gives younger air only in the mesosphere while tending to age the stratospheric air. Moreover, the H_2O change seems to be almost entirely responsible for rendering the northern hemispheric age/N_2O correlation more similar to the southern in 2060 than it is in 1995. Taken as a whole, these findings suggest that the extra H_2O in 2060 compared with 1995 has a systematically different effect on the general circulation than the extra CO_2 responsible for the bulk of the residual response. This may be a consequence either of the different radiative properties of the two gases, or of the CH_4-derived H_2O increase being spatially varying while the CO_2 increase is wholly uniform.

[49] The changed atmospheric conditions in 2060 lead to an increased prevalence of PSCs. Around 20% to 25% of the increase is due to the microphysical effect of the extra H_2O, with the remainder attributable to the lower temperature of the vortex. Although the more widespread PSCs cause a greater fractional release of reactive chlorine, a simple chemical treatment implies that this positive impact on chemical ozone destruction is outweighed by the negative impact of the reduced chlorine loading in 2060. Nevertheless, the H_2O increase does make the 2060 Arctic ozone loss ~15% greater than it would otherwise be.

[50] Overall, these results suggest that an H_2O increase stemming from a rise in tropospheric CH_4 could have a significant impact on the middle-atmospheric response to the changing radiative environment over the coming decades. Additionally, the study has revealed certain details of the H_2O action in the UM, notably the asymmetric effect on the general circulation, that invite comparative investigation in different modeling systems. Further work is also required to characterize the potential role of CH_4-derived H_2O over a broader range of future scenarios, and in the context of other potential sources of H_2O change.

[51] **Acknowledgments.** The H_2O chemical parameterization used here is a development of an earlier scheme written by P. A. Stott and A. Pardaens. Two-dimensional chemical reaction rates were supplied by Vicky West. The Cariolle ozone scheme was implemented in the UM by Peter Braesicke, and the finite volume tracer advection scheme was implemented by Andrew Gregory. This work was financially supported by the Natural Environment Research Council as part of the U.K. Universities Global Atmospheric Modelling Programme.

References

Abbas, M. M., et al. (1996), Seasonal variations of water vapor in the lower stratosphere inferred from ATMOS/ATLAS 3 measurements of H_2O and CH_4, *Geophys. Res. Lett.*, *23*, 2401–2404.

Austin, J. (2002), A three-dimensional coupled chemistry-climate model simulation of past stratospheric trends, *J. Atmos. Sci.*, *59*, 218–232.

Austin, J., and N. Butchart (1994), The influence of climate change and the timing of stratospheric warmings on Arctic ozone depletion, *J. Geophys. Res.*, *99*, 1127–1145.

Austin, J., N. Butchart, and K. P. Shine (1992), Possibility of an Arctic ozone hole in a doubled CO_2 climate, *Nature*, *360*, 221–225.

Austin, J., J. Knight, and N. Butchart (2000), Three-dimensional chemical model simulations of the ozone layer: 1979–2015, *Q. J. R. Meteorol. Soc.*, *126*, 1533–1566.

Austin, J., N. Butchart, and J. Knight (2001), Three-dimensional chemical model simulations of the ozone layer: 2015–55, *Q. J. R. Meteorol. Soc.*, *127*, 959–974.

Austin, J. N., et al. (2003), Uncertainties and assessments of chemistry-climate models of the stratosphere, *Atmos. Chem. Phys.*, *3*, 1–27.

Braesicke, P., and J. Pyle (2003), Changing ozone and changing circulation in northern mid-latitudes: Possible feedbacks?, *Geophys. Res. Lett.*, *30*(2), 1059, doi:10.1029/2002GL015973.

Butchart, N., J. Austin, J. R. Knight, A. A. Scaife, and M. L. Gallani (2000), The response of the stratospheric climate to projected changes in the concentrations of well-mixed greenhouse gases from 1992 to 2051, *J. Clim.*, *13*, 2142–2159.

Cariolle, D., and M. Deque (1986), Southern-hemisphere medium scale waves and total ozone disturbances in a spectral general-circulation model, *J. Geophys. Res.*, *91*, 10,825–10,846.

Carslaw, K. S., B. Luo, and T. Peter (1995), An analytic expression for the composition of aqueous HNO_3-H_2SO_4 stratospheric aerosols including gas phase removal of HNO_3, *Geophys. Res. Lett.*, *22*, 1877–1880.

Chabrillat, S., and G. Kockarts (1997), Simple parameterization of the absorption of the solar Lyman-alpha line, *Geophys. Res. Lett.*, *24*, 2659–2662.

Cullen, M. J. P. (1993), The unified forecast/climate model, *Meteorol. Mag.*, *122*, 81–94.

Cusack, S., A. Slingo, J. M. Edwards, and M. Wild (1998), The radiative impact of a simple aerosol climatology on the Hadley Centre atmospheric GCM, *Q. J. R. Meteorol. Soc.*, *124*, 2517–2526.

Dvortsov, V. L., and S. Solomon (2001), Response of the stratospheric temperatures and ozone to past and future increases in stratospheric humidity, *J. Geophys. Res.*, *106*, 7505–7514.

Edwards, J. M., and A. Slingo (1996), Studies with a flexible new radiation code. I: Choosing a configuration for a large-scale model, *Q. J. R. Meteorol. Soc.*, *122*, 689–719.

Forster, P. M. de F., and K. P. Shine (1999), Stratospheric water vapour changes as a possible contributor to observed stratospheric cooling, *Geophys. Res. Lett.*, *26*, 3309–3312.

Forster, P. M. de F., and K. P. Shine (2002), Assessing the climate impact of trends in stratospheric water vapor, *Geophys. Res. Lett.*, *29*(6), 1086, doi:10.1029/2001GL013909.

Gregory, D., G. J. Shutts, and J. R. Mitchell (1998), A new gravity wave drag scheme incorporating anisotropic orography and low-level wave breaking: Impact upon the climate of the UK Meteorological Office unified model, *Q. J. R. Meteorol. Soc.*, *124*, 463–494.

Hall, T. M., and A. R. Plumb (1994), Age as a diagnostic of stratospheric transport, *J. Geophys. Res.*, *99*, 1059–1070.

Haynes, P. H., C. J. Marks, M. E. McIntyre, and K. P. Shine (1991), On the ''downward control'' of extratropical diabatic circulations by eddy-induced mean zonal forces, *J. Atmos. Sci.*, *48*, 651–678.

Hurst, D. F., G. S. Dutton, P. A. Romashkin, P. R. Wamsley, F. L. Moore, and J. W. Elkins (1999), Closure of the total hydrogen budget of the

northern extratropical lower stratosphere, *J. Geophys. Res.*, *104*, 8191–8200.

Intergovernmental Panel on Climate Change (IPCC) (2001), *Climate Change 2001: The Scientific Basis*, edited by J. T. Houghton et al., Cambridge Univ. Press, New York.

Kinnersley, J. S., and R. S. Harwood (1993), An isentropic two-dimensional model with an interactive parameterization of dynamical and chemical planetary wave fluxes, *Q. J. R. Meteorol. Soc.*, *119*, 1167–1193.

Le Texier, H., S. Solomon, and R. R. Garcia (1988), The role of molecular hydrogen and methane oxidation in the water vapour budget of the stratosphere, *Q. J. R. Meteorol. Soc.*, *114*, 281–295.

MacKenzie, I. A., and R. S. Harwood (2000), Arctic ozone destruction and chemical-radiative feedback, *J. Geophys. Res.*, *105*, 9033–9051.

MacKenzie, I. A., R. S. Harwood, P. A. Stott, and G. C. Watson (1999), Radiative-dynamic effects of the Antarctic ozone hole and chemical feedback, *Q. J. R. Meteorol. Soc.*, *125*, 2171–2203.

Mahfouf, J. F., D. Cariolle, J.-F. Geleyn, and B. Timbal (1994), Response of the Meteo-France climate model to changes in CO_2 and sea surface temperature, *Clim. Dyn.*, *9*, 345–362.

Minschwaner, K., R. J. Salawitch, and M. B. McElroy (1993), Absorption of solar radiation by O_2: Implications for O_3 and lifetimes of N_2O, $CFCL_3$, and CF_2Cl_2, *J. Geophys. Res.*, *98*, 10,543–10,561.

Mote, P. W., K. H. Rosenlof, M. E. McIntyre, E. S. Carr, J. C. Gille, J. R. Holton, J. S. Kinnersley, H. C. Pumphrey, J. M. Russel III, and J. W. Waters (1996), An atmospheric tape recorder: The imprint of tropical tropopause temperatures on stratospheric water vapour, *J. Geophys. Res.*, *101*, 3989–4006.

Newman, P. A., E. R. Nash, and J. E. Rosenfield (2001), What controls the temperature of the Arctic stratosphere during the spring?, *J. Geophys. Res.*, *106*, 19,999–20,010.

Oinas, V., A. A. Lacis, D. Rind, D. T. Shindell, and J. E. Hanson (2001), Radiative cooling by stratospheric water vapour: Big differences in GCM results, *Geophys. Res. Lett.*, *28*, 2791–2794.

Oltmans, S. J., H. Vomel, D. J. Hofmann, K. H. Rosenlof, and D. Kley (2000), The increase in stratospheric water vapor from balloon-borne, frostpoint hygrometer measurements at Washington DC and Boulder, Colorado, *Geophys. Res. Lett.*, *27*, 3453–3456.

Pitari, G., S. Palermi, and G. Visconti (1992), Ozone response to a CO_2 doubling-results from a stratospheric circulation model with heterogeneous chemistry, *J. Geophys. Res.*, *97*, 5953–5962.

Pope, V. D., M. L. Gallani, P. R. Rowntree, and R. A. Stratton (2000), The impact of new physical parameterizations in the Hadley Centre climate model: HADAM3, *Clim. Dyn.*, *16*, 123–146.

Pumphrey, H. C. (1999), Validation of a new prototype water vapor retrieval for the UARS Microwave Limb Sounder, *J. Geophys. Res.*, *104*, 9399–9412.

Rind, D., R. Suozzo, N. K. Balachandran, and M. J. Prather (1990), Climate change and the middle atmosphere. Part I: The doubled CO_2 climate, *J. Atmos. Sci.*, *47*, 475–494.

Rind, D., D. T. Shindell, P. Lonergan, and N. K. Balachandran (1998), Climate change and the middle atmosphere. Part III: The doubled CO_2 climate revisited, *J. Clim.*, *11*, 876–894.

Rosenfield, J. E., A. R. Douglass, and D. B. Considine (2002), The impact of increasing carbon dioxide on ozone recovery, *J. Geophys. Res.*, *107*(D6), 4049, doi:10.1029/2001JD000824.

Rosenlof, K. H., et al. (2001), Stratospheric water vapor increases over the past half-century, *Geophys. Res. Lett.*, *28*, 1195–1198.

Shindell, D. (2001), Climate and ozone response to increased stratospheric water vapour, *Geophys. Res. Lett.*, *28*, 1551–1554.

Shindell, D. T., D. Rind, and P. Lonergan (1998), Increased polar stratospheric ozone losses and delayed eventual recovery owing to increasing greenhouse gas concentrations, *Nature*, *392*, 589–592.

Siskind, D. E., K. Minschwaner, and R. S. Eckman (1994), Photodissociation of O_2 and H_2O in the middle atmosphere: Comparison of numerical methods and impact on model O_3 and OH, *Geophys. Res. Lett.*, *21*, 863–866.

Smith, C. A., J. D. Haigh, and R. Toumi (2001), Radiative forcing due to trends in stratospheric water vapour, *Geophys. Res. Lett.*, *28*, 179–182.

Waugh, D. W. (1997), Elliptical diagnostics of stratospheric polar vortices, *Q. J. R. Meteorol. Soc.*, *123*, 1725–1748.

World Meteorological Organization (WMO) (1999), Scientific assessment of ozone depletion: 1998, *Rep. 44*, Global Ozone Res. and Monit. Proj., Geneva.

Zhong, W.-Y., and J. D. Haigh (2001), An efficient and accurate correlated-k parameterization of infrared radiative transfer for troposphere-stratosphere-mesosphere GCMs, *Atmos. Sci. Lett.*, *1*, doi:10.1006/asle.2000.0022.

R. S. Harwood and I. A. MacKenzie, School of GeoSciences (Meteorology), University of Edinburgh, James Clerk Maxwell Building, The King's Buildings, Edinburgh EH9 3JZ, UK. (harwood@met.ed.ac.uk; iam@met.ed.ac.uk)